6-6-2016

# Thermally Selective Formation of Subsurface Oxygen in Ag(111) and Consequent Surface Structure

Jonathan Derouin
*Loyola University Chicago*

Rachael G. Farber
*Loyola University Chicago*

Marie E. Turano
*Loyola University Chicago*

Erin V. Iski
*University of Tulsa*

Daniel Killelea
*Loyola University Chicago*, dkillelea@luc.edu



## Recommended Citation

Derouin, Jonathan; Farber, Rachael G.; Turano, Marie E.; Iski, Erin V.; and Killelea, Daniel. Thermally Selective Formation of Subsurface Oxygen in Ag(111) and Consequent Surface Structure. ACS Catalysis, 6, 7: 4640-4646, 2016. Retrieved from Loyola eCommons, Chemistry: Faculty Publications and Other Works, http://dx.doi.org/10.1021/acscatal.6b01239

Article

# Thermally Selective Formation of Subsurface Oxygen in Ag(111) and Consequent Surface Structure

Jonathan Derouin, Rachael G Farber, Marie E Turano, Erin Valentina Iski, and Daniel R Killelea

*ACS Catal.*, **Just Accepted Manuscript** • DOI: 10.1021/acscatal.6b01239 • Publication Date (Web): 06 Jun 2016

# Thermally Selective Formation of Subsurface Oxygen in Ag(111) and Consequent Surface Structure

Jonathan Derouin, Rachael G. Farber, Marie E. Turano, Erin V. Iski[†], and Daniel R. Killelea*

*Department of Chemistry & Biochemistry, Loyola University Chicago, 1068 W. Sheridan Rd., Chicago, IL 60660*

[†] *Department of Chemistry and Biochemistry, The University of Tulsa, 800 S. Tucker Dr., Tulsa, OK 74104*

***Revised Manuscript for ACS Catalysis***

*Corresponding Author. Email address: dkillelea@luc.edu ; ph: (773) 508-3136

## Abstract

A long-standing challenge in the study of heterogeneously catalyzed reactions on silver surfaces has been the determination of what oxygen species are of greatest chemical importance. This is due to the coexistence of several different surface phases on oxidized silver surfaces. A further complication is subsurface oxygen ($O_{sub}$). $O_{sub}$ are O atoms absorbed into the near surface of a metal, and are expected to alter the surface in terms of chemistry and structure, but these effects have yet to be well characterized. We studied oxidized Ag(111) surfaces after exposure to gas-phase O atoms to determine how $O_{sub}$ is formed and how its presence alters the resultant surface structure. Using a combination of surface science techniques to quantify $O_{sub}$ formation and the resultant surface structure, we observed that once 0.1 ML of $O_{sub}$ has formed, the surface dramatically, and uniformly, reconstructed to a striped phase at the expense of all other surface phases. Furthermore, $O_{sub}$ formation was hindered at temperatures above 500 K. The thermal dependence for $O_{sub}$ formation suggests that at industrial catalytic conditions of 475 – 500 K for the epoxidation of ethylene-to-ethylene oxide, $O_{sub}$ would be present and is a factor in the subsequent reactivity of the catalysts. These findings point to the need for the incorporation of $O_{sub}$ into catalytic models as well as further theoretical investigation of the resultant structure observed in the presence of $O_{sub}$.

## Introduction

It is well established that subsurface oxygen ($O_{sub}$) forms in the selvedge region of Ag(111) after exposure to gas-phase atomic oxygen (AO) (1), excess $NO_2$ (2), or high pressure $O_2$ exposures (3-4). What is far less clear is what factors enhance or disfavor the formation of $O_{sub}$, and furthermore, how the electronic and geometric structure of the surface is altered by $O_{sub}$. To date, most studies have focused on the formation of surface oxides and their structures (5-7), but quantification of $O_{sub}$ formation, until now, has received far less attention. In this paper, we show that the temperature of the Ag(111) sample is a key parameter in the formation of $O_{sub}$. Furthermore, over a narrow temperature range, less than 50 K, $O_{sub}$ formation goes from being highly favorable to completely disfavored. Finally, we show that the surface is rather sensitive to the presence of $O_{sub}$, and once the selvedge of the metal reaches a critical concentration of $O_{sub}$, the surface exhibits a striped structure that is very different from the other surface oxide reconstructions. These findings have direct consequences for our understanding of how electrophilic oxygen that is reactive toward ethylene epoxidation, may be formed and how the structure of a silver catalyst will evolve under conditions of high oxygen coverage.

Oxygen induced reconstructions of Ag(111) surfaces have been widely studied and debated for many years (8). Ag(111) surfaces exhibit a variety of different surface reconstructions induced by adsorbed oxygen ($O_{ad}$) (5, 9), along with several other oxide species (10-16). The primary motivation to study the O/Ag(111) system is silver's importance as an industrial partial oxidation catalyst (11, 17). Virtually all ethylene oxide (EO), an important intermediate in the production of plastics, glycols, and polyester, is produced by the partial oxidation of ethylene to EO over Ag catalysts (18). The industrial synthesis of formaldehyde by the oxidation of methanol also relies on Ag catalysts (19). In addition, silver oxide has also

shown potential in applications ranging from data storage to antimicrobial coatings (5). However, a causal link between surface preparation and surface oxide structure(s) remains undeveloped (5, 7). Furthermore, it is not altogether clear how the various surface structures are tied to the 'electrophilic oxygen' species believed to be active in the partial oxidation reactions (2). Recently, significant progress has been made in these two directions and subsurface oxygen is believed to be critically important (13-14, 20), which has motivated the present study.

Ag is readily oxidized at atmospheric and elevated pressures, but preparation of oxidized Ag(111) surfaces is not straightforward under ultra-high vacuum (UHV, $P < 1\times10^{-9}$ Torr) conditions. The sticking probability of $O_2$ on Ag(111) is very small, approximately $1\times10^{-6}$, and therefore, comparatively high pressures (1 Torr and above) are required to oxidize the surface and return the sample to UHV for analysis (21). To avoid these inconvenient high-pressure exposures, alternative oxidants have been employed in UHV to prepare oxidized Ag(111) surfaces. For example, $NO_2$ (6, 22) or gas-phase atomic oxygen (AO) (1, 23) will oxidize Ag(111) under conditions appropriate for returning the system to UHV conditions. Ozone has been used as an oxygen source in a limited number of studies, mostly for polycrystalline Ag (24-25). $O_3$ exposures at 1 atm pressure favored formation of rough surfaces of the bulk oxide, $Ag_2O$, as was also observed for high fluxes of AO on Ag(111) (1). In spite of the carefully controlled exposure conditions, a complex variety of surface structures and oxygen species have been observed and postulated using these oxidizing techniques. Oxygen species described by various authors have included chemisorbed oxygen (21, 26), which is both weakly and strongly bound to the surface (27-28), $O_\gamma$ (29), nucleophilic and electrophilic oxygen (12), oxygen in the bulk, and $O_{sub}$ (4, 26, 30). The surface structures thus far identified or proposed include $p(4\times4)$ (9, 31), $c(3\times5\sqrt{3})$, $p(4\times5\sqrt{3})$ (32), (7x$\sqrt{3}$) (2), $c(4\times8)$ (7), $p(\sqrt{3}\times3\sqrt{3})R30°$ (33), and striped (7, 32)

structures as well as *p*(7×7) (34), AgO, and $Ag_2O$ oxide structures (1). As yet, there is little correlation between the oxidant, temperature, or flux, and the resultant surface structure. It seems that many of the structures are nearly isoenergetic, as reported in Density Functional Theory (DFT) calculations, and often have very similar stoichiometry (5), further complicating efforts at unraveling the structure-reactivity of oxidized silver surfaces.

Of the oxygen induced Ag surface reconstructions, the *p*(4×4) reconstruction of the (111) surface has been the most widely studied and is believed to be the most stable structure under conditions relevant for EO catalysis (10, 35). Rovida *et al*. first observed a *p*(4×4) low energy electron diffraction (LEED) pattern after dosing a Ag(111) crystal with high pressure $O_2$ in the early 1970's (36-37). Over the next thirty years, a variety of models for a *p*(4×4)-O/Ag structure were proposed and subsequently improved upon (38). In 2006, a model based on two Ag hexamer triangles separated by furrows containing oxygen atoms was proposed by the groups of Besenbacher (9) and Varga (31), as illustrated in Figure 1. Further studies over the past decade have further validated this model (8, 39). Two other surface reconstructions, the *c*(3×5√3) and *p*(4×5√3), are minor structural rearrangements of the *p*(4×4) structure and have been observed with scanning tunneling microscopy (STM) to coexist on oxidized Ag(111) (9, 32). Like the *p*(4×4) structure, the *c*(3×5√3) structure is also composed of hexameric Ag triangles separated by furrows containing O atoms, also illustrated in Figure 1, but the orientation of the triangles is different from the *p*(4×4). The unit cell for the *p*(4×5√3) structure contains two of the hexameric triangles, but also contains two decamer Ag triangles. The oxygen coverage is slightly higher for this reconstruction, 0.4 ML, as compared to 0.375 ML O for the *p*(4×4) or *c*(3×5√3) structures. In a series of STM measurements of oxidized Ag(111), Schnadt *et al.* observed two additional surface oxide structures that appear to not contain hexamer or decamer triangles (7). They

proposed a *c*(4×8) model for one structure, but were unable to determine the structure of the other, labeling it a stripe pattern. The stripe pattern observed by Schnadt *et al.* was significantly different from the stripe pattern observed by Carlisle *et al.* (32) in 2000, which was most likely *p*(4×5√3) structures within *p*(4×4) domains. The model for the *c*(4×8) structure was later revised (5); DFT calculations predict that this structure has a higher O coverage (0.5 ML) than the *p*(4×4) (0.375 ML), *c*(3×5√3) (0.4 ML), or *p*(4×5√3) (0.375 ML) structures.

Despite the identification of multiple O/Ag(111) surface structures, the active O species for ethylene epoxidation is still debated in terms of location and identity. In addition to surface oxygen (3), surface defects (40), subsurface oxygen (13, 41-42), and surface oxides (43-44) have all been proposed as factors in the selectivity of Ag catalyzed ethylene epoxidation. Unlike $NO_2$, which only forms *p*(4×4) domains and does not lead to subsurface O, AO exposure forms a variety of surface structures and $O_{sub}$. Herein, we report the results from a study of Ag(111) oxidized by AO under UHV conditions and show that the formation of $O_{sub}$ is greatly diminished by a slight (< 50 K) increase in the temperature of the silver solid during exposure. We further demonstrate that $O_{sub}$ has a pronounced effect on the surface structure and show the evolution of the surface structure with increasing coverage at several different sample temperatures. These findings have a direct impact on the heterogeneously catalyzed transformation of ethylene to ethylene oxide as the assumption of the predominance of the *p*(4×4) reconstruction is likely incomplete; in actuality, several structures coexist. Furthermore, the low temperatures used for epoxidation are likely required because the formation of subsurface oxygen is favored below 500 K; at higher temperatures, $O_{sub}$ is depleted and the necessary alteration of the surface induced by $O_{sub}$ that favors partial oxidation (41) is absent.

**Experimental Details**

Experiments were performed in an ultrahigh-vacuum scanning tunneling microscope (UHV-STM) apparatus described previously (45). A Ag(111) crystal (Surface Preparation Laboratory) was mounted on a flag-style Ta sample holder. The temperature was measured with a type-K thermocouple welded to the crystal. The surface was cleaned with repeated cycles of $Ar^+$ sputtering and annealing at 750 K until surface impurities were below the detection limit of the Auger electron spectrometer (AES). Surface cleanliness and order were verified by a sharp (1×1) low energy electron diffraction (LEED) pattern and imaging with STM.

The Ag(111) crystal was exposed to gas-phase atomic oxygen generated by dissociating $O_2$ (*g*) over a hot Ir filament. The filament was heated to 1750 K by passing 2.8 A at 1.6 VAC through the 0.25 mm diameter Ir wire in the UHV chamber. The chamber was backfilled with $O_2$ (*g*) to $5\times10^{-7}$ Torr. During exposure, the filament was brought within ≈ 0.5 cm from the front face of the Ag(111) crystal and the sample temperature was held constant at the deposition temperature ($T_{dep}$). After exposure, only oxygen was observed to accumulate on the surface, as reported previously (1). Once the AO exposure was completed, the sample was cooled to either 425 K for TPD and LEED analysis, or to 90 K for insertion into the STM chamber. For STM imaging, the manipulator was used to move the chilled sample to the STM chamber where a wobble stick was used to insert the sample into the STM. Once inserted, the STM was allowed to cool to the imaging temperature of 20 K. During imaging, there was negligible accumulation of background gases (46), and the oxidized surfaces were not altered, as confirmed by post-imaging TPD measurements. LEED measurements were performed at room temperature, and similarly, TPD spectra were unchanged by the LEED analysis. All TPD measurements were performed with a ramp rate of 3 K $s^{-1}$.

**Results and Discussion**

Both AO and $NO_2$ oxidize Ag(111) surfaces. Whereas AO exposures yield surfaces with both adsorbed oxygen ($O_{ad}$) and $O_{sub}$, only $O_{ad}$ results from $NO_2$ exposures for $T_{dep}$ = 500 K (6, 22). For these reasons, $NO_2$ oxidation provides a convenient calibration method for the uptake of oxygen during AO exposures. The Ag(111) sample was exposed to $NO_2$ from a directed doser at $T_{dep}$ = 500 K. After a 60 s exposure, TPD spectra showed a single desorption peak at T = 595 K, corresponding to the decomposition of the *p*(4x4) surface oxide with a coverage of $\theta_O$ = 0.375 ML (5), and the peak intensity was unchanged by longer exposures, suggesting the surface was fully covered by the reconstructed surface under these conditions. LEED analysis of the $NO_2$ dosed surface showed a sharp (4×4) pattern, and STM imaging exclusively found *p*(4×4) structures on the surface when the $NO_2$ exposure was performed at 500 K or higher. The integral of this peak was then used to determine the coverages for the AO exposures.

*Surface Temperature Effect on Oxygen Uptake on Ag(111)*

Figure 2 shows TPD data after exposing Ag(111) to AO for various exposure times with $T_{dep}$ = 475 K, 490 K, 500 K, 510 K, and 525 K. For all of the TPD spectra, the sharp peak at 595 K is from the decomposition of the surface reconstruction (6, 22). Additionally, no peaks were observed at higher desorption temperatures. A filament temperature of 1750 K was employed for all exposures and no higher temperature desorption peaks due to the formation of bulk oxide ($Ag_2O$) (1) on the surface or strongly-bound subsurface oxygen (2) were observed. In the TPD spectra for $T_{dep}$ = 525 K, only the single peak corresponding to the surface oxide was observed. The growth of the intensity of the peak slowed after 120 s AO exposure and at 300 s the peak became saturated; the desorption spectrum after the 600 s AO exposure was nearly identical and overlaps the 300 s exposure desorption peak. The saturation of the desorption peak indicates that additional AO did not stick to the surface. The desorption spectra for the $T_{dep}$ = 510 K were

similarly dominated by the 595 K surface reconstruction decomposition peak that also saturated after 300 s exposure. However, a small feature was observed just below 550 K after the 300 s and, to a lesser extent, the 600 s exposures. This small peak was more pronounced in the TPD spectra for $T_{dep}$ = 500 K, and the peak intensity increased for lower deposition temperatures. For $T_{dep}$ = 490 K and 475 K, the lower temperature peak continued to grow with exposure, and its peak intensity, as well as the corresponding temperature, gradually increased until it overwhelmed the surface desorption peak, as seen in Figure 2E for $T_{dep}$ = 475 K.

The most likely explanation for the lower temperature desorption peak near 550 K in Fig. 2 C-E is $O_{sub}$. Previous reports showed that *bulk* oxygen desorbs from Ag in a broad peak from 600 K to > 800 K (47). However, $O_{sub}$, which are dissolved O atoms in the selvedge of the metal, has been shown to desorb from Ag at temperatures around 580 K, below that of the surface oxide at 595 K (4, 21, 48). As observed both in a previous report (1) and in the present study, Rehren, *et al*. found that the lower-temperature TPD peak corresponding to desorption of $O_{sub}$ did not saturate with exposure, whereas the surface peak did (47). $O_{sub}$ desorbs at a lower temperature because it is thermodynamically unstable with respect to surface adsorbed oxygen. Calculations show that the several surface oxides and reconstructions have similar surface free energies, and they are more stable than $O_{sub}$ around 600 K (5, 20, 49), therefore, $O_{sub}$ desorbs before decomposition of the surface reconstruction. This behavior is qualitatively similar to subsurface H ($H_{sub}$) on Ni(111), where $H_{sub}$ is metastable with respect to adsorbed H ($H_{ad}$) and desorbs at around 100 K lower temperature than $H_{ad}$ (50-51).

Figure 3A shows TPD spectra for 300 s AO exposures at five different deposition temperatures along with desorption spectra after saturation dosing with $NO_2$ yielding $\theta_O$ = 0.375 ML. From Figure 3A, it is clear that substantially more than $\theta_O$ = 0.375 ML of $O_2$ desorbed after

dosing for 300s with $T_{dep} \leq 500$ K. As Figure 3B shows, with extended dosing at lower temperatures, desorption of the more than 1.0 ML of $O_2$ was observed. Such high coverages are not consistent with any known or predicted surface structures suggesting that oxygen is desorbing from the subsurface or from adsorption on top of surface oxide structures similar to O on Pd (52). Again, $O_{sub}$ is the plausible explanation. In addition to the fact that more than the equivalent of 1.0 ML of $O_2$ desorbs, the assignment of the peak to $O_{sub}$ is supported by the apparent zero order shape of the peak. A common leading edge with the peak maximum shifting to higher temperatures, as shown in Figures 2C-E and 3A, is characteristic of zero order desorption kinetics (53). Because oxygen desorbs from Ag(111) as a molecule rather than an atomic species, recombination must take place prior to desorption and therefore, true zero order desorption is not possible. However, recombinative desorption leading to pseudo-zero order peaks has been reported for other surfaces (50, 54-55). The shape of the lower temperature desorption peak was most likely due to the surface coverage-independent emergence of oxygen from the subsurface in a zero order process. Emergent O atoms from the subsurface transiently adsorb onto unstable surface sites before rapidly reacting with $O_{ad}$ or other emergent O atoms. This analysis is further supported by a closer examination of the peaks in Figure 3A. When the lower temperature peak was present, the surface oxygen desorption peak was slightly larger than the saturated $NO_2$ surface desorption peak. This is consistent with some O atoms emerging from the surface and replacing the O atoms desorbed from surface oxide phases.

It is clear from Figure 3B that for $T_{dep} \geq 500$ K, the uptake of O on the Ag(111) surface reached a limiting coverage. This was likely because the surface oxide grew until it extended across the entire surface, and $O_{sub}$ was unstable. However, for $T_{dep} < 500$ K, O continued to stick even after the surface oxide peak saturates, and the sticking was favored at lower temperatures.

As discussed, this lower temperature peak (Figure 3A) was caused by the emergence of $O_{sub}$ and the subsequent recombinative desorption of $O_2$ (1, 47). Due to the pronounced temperature dependence of the peak intensity, $O_{sub}$ formation was clearly hindered for exposure temperatures above 500 K. In contrast, for $T_{dep}$ below 500 K, uptake continued, suggesting $O_{sub}$ was stable at 475 K, and slightly less so at 490 K. The decrease in oxygen desorption cannot be explained by desorption due to the elevated $T_{dep}$ alone. For example, a 600 s AO exposure at $T_{dep}$ = 475 K yielded 1.2 ML O. When $T_{dep}$ was increased to 500 K, the O uptake was 0.42 ML, and the desorption spectra was dominated by surface O with a small lower temperature peak corresponding to $O_{sub}$. From the TPD data, at 500 K, $\frac{d\theta_O}{dt} = 1.8\times10^{-5}$ ML $s^{-1}$, so only a 0.015 ML decrease in O desorption would be anticipated, rather than the nearly 0.8 ML decrease observed. This confirms that desorption due to elevated $T_{dep}$ is insufficient to explain the reduction in O uptake. For all experiments, after the exposure was completed, the crystal was immediately cooled below 425 K.

It is worth noting that the $O_{sub}$ observed here is a different species than the 'strongly-bound' subsurface oxygen, or bulk oxygen, formed at exposure temperatures greater than 650 K (2). It turns out that the barrier for diffusion from the subsurface to the bulk is greater than the barrier for diffusion from the subsurface to the surface (49), therefore requiring elevated temperatures to activate the penetration of O into the bulk. In the present study, we observed that under modest fluxes of incident O atoms, dissolved O formation was hindered at temperatures above 500 K, so correspondingly, the higher dosing temperatures required to form bulk oxygen in earlier TPD studies preclude the presence of $O_{sub}$. When an Ag surface is exposed to gas-phase O atoms, the selvedge is likely populated with $O_{sub}$ during exposure; because of the modest temperature, the $O_{sub}$ atoms lack the energy to diffuse into the bulk, and

remain trapped in the near surface region. Alternatively, when Ag surfaces are exposed to $O_2$ under high-temperature, high-pressure conditions, dissolved O forms directly from surface species (56), which can then diffuse into the bulk.

*Evolution of Surface Structure with $O_{sub}$ Abundance*

The surface structures for varying total coverages of O were determined using LEED and STM. These methods are considered complimentary in that LEED provides a global diffraction pattern that shows an average structure, while STM provides an atomic-scale image map of the local surface structure. Interpretation of the LEED pattern is facilitated by comparison to STM images obtained at several different positions across the surface (separated by a few μm). In the case where a single, clean LEED pattern is observed, and the STM images also show little structural variation, it is reasonable to infer that the surface is covered with the structure corresponding to that LEED pattern. Alternatively, a complicated LEED pattern and STM images showing the coexistence of different surface structures indicates that the surface is inhomogeneous, and there is no single representative surface structure. In this study of the surface structure of Ag(111) after AO oxidation, we found that prolonged exposure often results in a single, dominant phase, but intermediate exposures result in several phases coexisting on the surface. We also saw that high concentrations ($\theta_{O,\,sub} \geq 0.1$ ML) of subsurface oxygen induce a new surface phase that covers the entire surface in a single domain.

Figure 4 shows representative LEED patterns taken after exposing the Ag(111) sample to AO for 30 s or 600 s, at either $T_{dep}$ = 525 K or 490 K. After the 30 s exposures, the patterns were very similar for both $T_{dep}$ = 525 K and 490 K. As the exposure increased, the evolution of the LEED patterns for the two $T_{dep}$ diverged. At $T_{dep}$ = 525 K, the LEED pattern for the 600 s exposure did not appear to fluctuate significantly from the 30 s exposure. The pattern appeared

to sharpen and the (1×1) pattern from the underlying Ag(111) faded, which suggests that patches of a single surface oxide structure formed initially, and the entire surface became covered in that single structure with increasing exposure. On the other hand, at $T_{dep}$ = 490 K, the LEED pattern changed with increasing AO exposure, and for 300 s and longer exposures, a striped pattern, shown in Figure 4D, became predominant. At exposures between 30 s and 300 s, the LEED pattern became complex, indicating several structures were present on the surface. It is interesting to note that the *p*(4×4) pattern was not predominant at any exposure. In complicated LEED patterns (*e.g.* Figure 4C), faint (4×4) patterns were seen, but they were never particularly bright. When the Ag(111) crystal was exposed to $NO_2$ to oxidize the surface, only the (4×4) pattern was observed, as reported previously for $NO_2$ and $O_2$ oxidation (6, 37).

Although we are presently unable to provide a detailed analysis of the LEED pattern obtained for higher $O_{sub}$ concentrations (Figure 4 lower right), some qualitative properties are useful to highlight. The stripes retain the 60° angle characteristic of commensurate structures on FCC (111) surfaces. Additionally, the spacing between the spots in the stripes is significantly less than the separation between the stripes. There appears to be a repeating unit of either 6 or 12 spots, somewhat regularly spaced, between the stripes. This data suggests that the surface features giving the diffraction pattern have a single nearest neighbor spacing (reciprocal of stripe spacing), while the longer-range structure (reciprocal of the spot separation) is less regular.

The oxidized Ag(111) surfaces were imaged using STM for different combinations of $T_{dep}$ and AO exposure to determine the structures formed for each set of conditions. The LEED patterns were used as guides for interpretation of the STM images. With $NO_2$ oxidation, only the *p*(4×4)-O surface oxide reconstruction was observed for $T_{dep} \geq 500$ K, and the surface was

uniformly covered with this structure. With the single LEED pattern, this confirmed the use of the TPD integral as the standard for 0.375 ML O on the Ag(111) surface.

At higher AO deposition temperatures, specifically at $T_{dep}$ = 525 K, a single surface reconstruction structure, $p(4\times5\sqrt{3})$, was observed to uniformly cover the Ag(111) surface over the course of time. STM images after AO dosing at $T_{dep}$ = 525 K are shown in Figure 5. After dosing for less than 60 s, the surface has large domains of $p(4\times5\sqrt{3})$ (Figure 5A) and large areas of bare Ag with chemisorbed O, which appear as randomly scattered dark spots (Figure 5B). The presence of bare Ag(111) with scattered chemisorbed O interspersed with ordered domains of $p(4\times5\sqrt{3})$ is consistent with the LEED patterns seen in Figure 4. The Ag(111) displayed the characteristic hexagonal diffraction pattern, while the $p(4\times5\sqrt{3})$ structure resulted in the faint additional decorations in the LEED image, suggestive of the introduction of a long-range ordered surface structure. As the AO exposure increased over time, the entire surface was covered with the surface oxide. The principal structure was the $p(4\times5\sqrt{3})$ reconstruction, but areas of the $c(3\times5\sqrt{3})$ structure were also found. However, eventually the surface was predominately covered by $c(3\times5\sqrt{3})$ structures with bands of $p(4\times5\sqrt{3})$ structures as shown by the 600 s exposure image, Figure 5D. The oxygen coverages for the two structures were very close, 0.375 ML for $p(4\times5\sqrt{3})$ versus 0.4 ML for $c(3\times5\sqrt{3})$, and either case indicates that the surface was saturated with oxygen. The TPD data supports this statement, because the peak intensity did not increase from 300 s to 600 s. Furthermore, despite the principal surface structure shifting from $p(4\times5\sqrt{3})$ to $c(3\times5\sqrt{3})$, there were very little changes in the observed LEED pattern. Taken together, this demonstrates that at 525 K, subsurface oxygen formation was eliminated and large homogeneous domains of a single surface reconstruction were formed.

When the Ag(111) sample was exposed to AO at $T_{dep}$ = 490 K, the resultant surfaces were initially inhomogeneous, but after continued exposure, the surfaces became dominated by large homogeneous domains of a striped pattern. Figure 6 shows STM images taken after several AO exposures and these images demonstrate how the surface structure evolved with increasing AO exposure. Initially, uptake was similar to what was seen at elevated temperature, but once intermediate exposures were reached, the surfaces were markedly different. After 30 s AO exposure (Figure 6A) at 490 K, the surface had patches of the $p(4\times5\sqrt{3})$ surface reconstruction, but was largely clean Ag(111) and chemisorbed O atoms. As the AO exposure increased, no single surface structure became predominant. Instead, a few different surface reconstructions were observed to coexist, and interestingly, these domains had different oxygen coverages. For example, after a 120 s AO exposure at $T_{dep}$ = 490 K (Figure 6 C and D), areas of $p(4\times4)$-O, $c(3\times5\sqrt{3})$-O, and $p(4\times8)$-O were observed. The first two structures have $\theta_O$ = 0.375 ML, but the $p(4\times8)$-O structure corresponds to $\theta_O$ = 0.5 ML. Due to the atomic-level spatial resolution that is possible with STM imaging measurements, small domains of varying surface structures were identified. While the TPD spectra averages the total amount of O for the whole Ag(111) surface, STM allows for the very precise, local analysis of the Ag(111) surface. These STM images revealed the coexistence of multiple surface structure domains and, as a result, show local variations in the oxygen surface coverage. The coverage of the $p(4\times8)$-O structure increased with exposure, but several domains were always observed. However, after 300 s AO exposures, the surface structure homogenized to a single, striped, structure. For AO exposures with $T_{dep}$ < 500 K, and for longer than 300 s, the entire surface was observed to be covered with a striped pattern (Figure 6 E and F). Small patches of this pattern were previously reported by Besenbacher's group (7), but it has not been previously observed to be particularly common,

much less covering the entire surface completely. A closer look at the STM images of the surface after a 300 s AO exposure, shown in Figure 6E, reveals an intermixing of thin and thick stripes across the terrace. Presently, we have been unable to further resolve these features, but they qualitatively agree with the LEED images. The key detail from these STM images is that the surface adopts the striped pattern after subsurface oxygen forms as indicated by the TPD spectra. This indicates that $O_{sub}$ induces the striped pattern, disrupting the previously observed surface reconstructions. The effect occurs once the abundance of $O_{sub}$ exceeds 0.1 ML (total $\theta_O$ > 0.5 ML).

**Conclusion**

Subsurface oxygen distorts the surface structures of oxidized Ag(111) surfaces. This effect is moderated by the temperature of the silver surface during the exposure to atomic oxygen. At exposure temperatures above 500 K, subsurface oxygen formation was hindered, and the oxygen was found only on the surface in well-ordered surface oxide reconstructions. On the other hand, when the Ag(111) surface was oxidized below 500 K, subsurface oxygen was formed, and when the coverage was ~ 0.1 ML $O_{sub}$, a striped pattern was observed across the surface. These findings are relevant to the heterogeneously catalyzed transformation of ethylene over silver catalysts. Industrially, these reactions are run close to 500 K, which is right on the dividing line for subsurface oxygen stability and therefore, subsurface oxygen is an important factor in the structural and chemical nature of the surface and must be included in accurate models of silver-catalyzed reactions.

**Acknowledgements**

Acknowledgment is made to the Donors of the American Chemical Society Petroleum Research Fund for partial support of this research through Grant PRF #54770-DNI5. This work was also

supported by the College of Arts and Sciences at Loyola University Chicago. J. Derouin wishes to thank the Schmitt Foundation for an Arthur J. Schmitt Dissertation Fellowship. M.E. Turano would like to thank Loyola University for a Provost's Fellowship and Mulcahy Scholarship. E.V. Iski acknowledges the Department of Chemistry and Biochemistry at the University of Tulsa for their support. We would also like to thank S. Alex Kandel for use of the LEED.

## References


(1) Derouin, J.; Farber, R. G.; Heslop, S. L.; Killelea, D. R., *Surf. Sci.* **2015,** *641*, L1-4.
(2) Boecklein, S.; Guenther, S.; Wintterlin, J., *Angewandte Chemie-International Edition* **2013,** *52*, 5518-5521.
(3) Bukhtiyarov, V. I.; Havecker, M.; Kaichev, V. V.; Knop-Gericke, A.; Mayer, R. W.; Schlogl, R., *Phys. Rev. B* **2003,** *67*, 235422.
(4) Vattuone, L.; Savio, L.; Rocca, M., *Phys. Rev. Lett.* **2003,** *90*.
(5) Martin, N. M.; Klacar, S.; Gronbeck, H.; Knudsen, J.; Schnadt, J.; Blomberg, S.; Gustafson, J.; Lundgren, E., *J. Phys. Chem. C* **2014,** *118*, 15324-15331.
(6) Bare, S. R.; Griffiths, K.; Lennard, W. N.; Tang, H. T., *Surf. Sci.* **1995,** *342*, 185-198.
(7) Schnadt, J.; Knudsen, J.; Hu, X. L.; Michaelides, A.; Vang, R. T.; Reuter, K.; Li, Z.; Laegsgaard, E.; Scheffler, M.; Besenbacher, F., *Phys. Rev. B* **2009,** *80*, 075424.
(8) Reichelt, R.; Guenther, S.; Wintterlin, J., *J. Chem. Phys.* **2007,** *127*.
(9) Schnadt, J.; Michaelides, A.; Knudsen, J.; Vang, R. T.; Reuter, K.; Laegsgaard, E.; Scheffler, M.; Besenbacher, F., *Phys. Rev. Lett.* **2006,** *96*.
(10) Jones, T. E.; Rocha, T. C. R.; Knop-Gericke, A.; Stampfl, C.; Schlogl, R.; Piccinin, S., *Phys. Chem. Chem. Phys.* **2015,** *17*, 9288-9312.
(11) Rocha, T. C. R.; Oestereich, A.; Demidov, D. V.; Havecker, M.; Zafeiratos, S.; Weinberg, G.; Bukhtiyarov, V. I.; Knop-Gericke, A.; Schlogl, R., *Phys. Chem. Chem. Phys.* **2012,** *14*, 4554-4564.
(12) Kaichev, V. V.; Bukhtiyarov, V. I.; Havecker, M.; Knop-Gercke, A.; Mayer, R. W.; Schlogl, R., *Kinet. Catal.* **2003,** *44*, 432-440.
(13) Greeley, J.; Mavrikakis, M., *J. Phys. Chem. C* **2007,** *111*, 7992-7999.
(14) Jones, T. E.; Rocha, T. C. R.; Knop-Gericke, A.; Stampfl, C.; Schloegl, R.; Piccinin, S., *Acs Catalysis* **2015,** *5*, 5846-5850.
(15) Jones, T. E.; Rocha, T. C. R.; Knop-Gericke, A.; Stampfl, C.; Schloegl, R.; Piccinin, S., *Phys. Chem. Chem. Phys.* **2015,** *17*, 9288-9312.
(16) Bao, X.; Muhler, M.; Schedel-Niedrig, T.; Schlogl, R., *Phys. Rev. B* **1996,** *54*, 2249-2262.
(17) de Leeuw, N. H.; Nelson, C. J., *J. Phys. Chem. B* **2003,** *107*, 3528-3534.
(18) Ishikawa, A.; Nakatsuji, H., *J. Comput. Chem.* **2013,** *34*, 1828-1834.
(19) Wachs, I. E., *Surf. Sci.* **2003,** *544*, 1-4.
(20) Li, W. X.; Stampfl, C.; Scheffler, M., *Phys. Rev. B* **2003,** *67*.
(21) Campbell, C. T., *Surf. Sci.* **1985,** *157*, 43-60.
(22) Huang, W. X.; White, J. M., *Surf. Sci.* **2003,** *529*, 455-470.
(23) Li, L.; Yang, J. C., *Mater. High Temp.* **2003,** *20*, 601-606.
(24) Wiesinger, R.; Grayburn, R.; Dowsett, M.; Sabbe, P. J.; Thompson, P.; Adriaens, A.; Schreiner, M., *J. Anal. At. Spectrom.* **2015,** *30*, 694-701.
(25) Waterhouse, G. I. N.; Bowmaker, G. A.; Metson, J. B., *Appl. Surf. Sci.* **2001,** *183*, 191-204.
(26) Grant, R. B.; Lambert, R. M., *Surf. Sci.* **1984,** *146*, 256-268.
(27) Bao, X.; Muhler, M.; Pettinger, B.; Uchida, Y.; Lehmpfuhl, G.; Schlogl, R.; Ertl, G., *Catal. Lett.* **1995,** *32*, 171-183.
(28) Reichelt, R.; Gunther, S.; Wintterlin, J., *J. Phys. Chem. C* **2011,** *115*, 17417-17428.
(29) Bao, X.; Muhler, M.; Pettinger, B.; Schlogl, R.; Ertl, G., *Catal. Lett.* **1993,** *22*, 215-225.

(30) Savio, L.; Vattuone, L.; Rocca, M., *Applied Physics a-Materials Science & Processing* **2007,** *87*, 399-404.
(31) Schmid, M.; Reicho, A.; Stierle, A.; Costina, I.; Klikovits, J.; Kostelnik, P.; Dubay, O.; Kresse, G.; Gustafson, J.; Lundgren, E.; Andersen, J. N.; Dosch, H.; Varga, P., *Phys. Rev. Lett.* **2006,** *96*.
(32) Carlisle, C. I.; Fujimoto, T.; Sim, W. S.; King, D. A., *Surf. Sci.* **2000,** *470*, 15-31.
(33) Bao, X.; Barth, J. V.; Lehmpfuhl, G.; Schuster, R.; Uchida, Y.; Schlogl, R.; Ertl, G., *Surf. Sci.* **1993,** *284*, 14-22.
(34) Reicho, A.; Stierle, A.; Costina, I.; Dosch, H., *Surf. Sci.* **2007,** *601*, L19-L23.
(35) Ozbek, M. O.; van Santen, R. A., *Catal. Lett.* **2013,** *143*, 131-141.
(36) Rovida, G.; Pratesi, F.; Magliett.M; Ferroni, E., *J. Vac. Sci. Technol.* **1972,** *9*, 796-798.
(37) Rovida, G.; Pratesi, F.; Magliett.M; Ferroni, E., *Surf. Sci.* **1974,** *43*, 230-256.
(38) Michaelides, A.; Reuter, K.; Scheffler, M., *J. Vac. Sci. Technol. A* **2005,** *23*, 1487-1497.
(39) Klust, A.; Madix, R. J., *J. Chem. Phys.* **2007,** *126*.
(40) Bal'zhinimaev, B. S., *Kinet. Catal.* **1999,** *40*, 795-810.
(41) Grant, R. B.; Lambert, R. M., *J. Catal.* **1985,** *92*, 364-375.
(42) van Santen, R. A.; de Groot, C. P. M., *J. Catal.* **1986,** *98*, 530 - 539.
(43) Bocquet, M. L.; Sautet, P.; Cerda, J.; Carlisle, C. I.; Webb, M. J.; King, D. A., *J. Am. Chem. Soc.* **2003,** *125*, 3119-3125.
(44) Michaelides, A.; Bocquet, M. L.; Sautet, P.; Alavi, A.; King, D. A., *Chem. Phys. Lett.* **2003,** *367*, 344-350.
(45) Derouin, J.; Farber, R. G.; Killelea, D. R., *J. Phys. Chem. C* **2015,** *119*, 14748-14755.
(46) Kolb, M. J.; Farber, R. G.; Derouin, J.; Badan, C.; Calle-Vallejo, F.; Juurlink, L. B. F.; Killelea, D. R.; Koper, M. T. M., *Phys. Rev. Lett.* **2016,** *116*.
(47) Rehren, C.; Isaac, G.; Schlogl, R.; Ertl, G., *Catal. Lett.* **1991,** *11*, 253-265.
(48) Bukhtiyarov, V. I.; Kaichev, V. V., *Journal of Molecular Catalysis a-Chemical* **2000,** *158*, 167-172.
(49) Todorova, M.; Li, W. X.; Ganduglia-Pirovano, M. V.; Stampfl, C.; Reuter, K.; Scheffler, M., *Phys. Rev. Lett.* **2002,** *89*.
(50) Ceyer, S. T., *Acc. Chem. Res.* **2001,** *34*, 737-744.
(51) Killelea, D. R.; Campbell, V. L.; Shuman, N. S.; Utz, A. L., *Science* **2008,** *319*, 790-793.
(52) Kan, H. H.; Shumbera, R. B.; Weaver, J. F., *Surf. Sci.* **2008,** *602*, 1337-1346.
(53) Dashbach, J. P., B; Smith, R. S; Kay, B;, *J. Chem. Phys.* **2003,** *120*, 1516-1523.
(54) Stojilovic, N.; Ramsier, R. D., *Appl. Surf. Sci.* **2006,** *252*, 5839-5845.
(55) Henderson, M.; Joyce, S.; Rustad, J., *Surf. Sci.* **1998,** *417*, 66-81.
(56) Qu, Z. P.; Cheng, M. J.; Huang, W. X.; Bao, X. H., *J. Catal.* **2005,** *229*, 446-458.

**Figure 1**

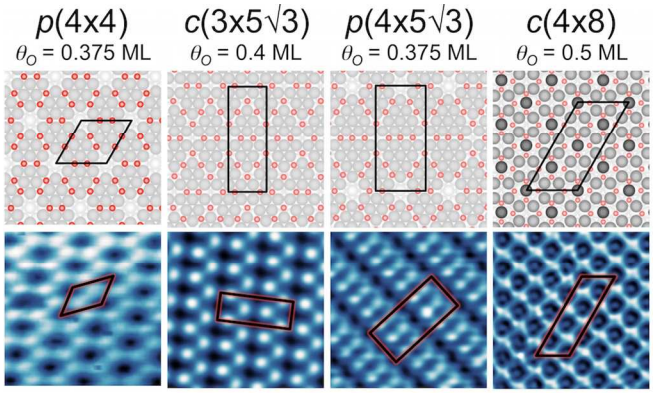


**Figure 1:** Illustrations of the four principal surface oxide reconstructions observed. From left to right, *p*(4×4)-O, *c*(3×5√3)-O, *p*(4×5√3)-O, and *c*(4×8)-O. In each illustration, red balls depict O atoms, darker gray the surface Ag atoms, and the light gray balls depict the topmost layer of the underlying Ag(111). Beneath each illustration is a 5 nm × 5 nm STM image of the corresponding surface. Surface unit cells are shown by black tetragons.

**Figure 2**

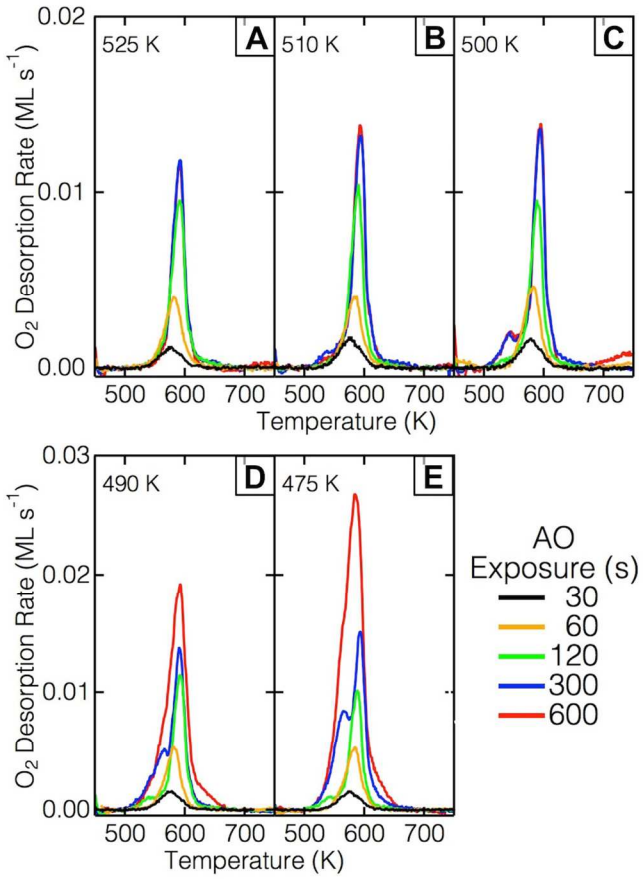


**Figure 2:** TPD spectra after exposure of Ag(111) to AO at five different temperatures, A) $T_{dep}$ = 525 K, B) $T_{dep}$ = 510 K, C) $T_{dep}$ = 500 K, D) $T_{dep}$ = 490 K, and E) $T_{dep}$ = 475 K . For each, the Ir filament was at 1750 K and the background pressure of $O_2$ was 5.0 $\times 10^{-7}$ Torr. The surface oxide peak at 595 K saturates after 300 s (blue traces) for all $T_{dep}$, but the lower temperature peak near 550 K increases with exposure time for $T_{dep}$ below 500 K.

**Figure 3**

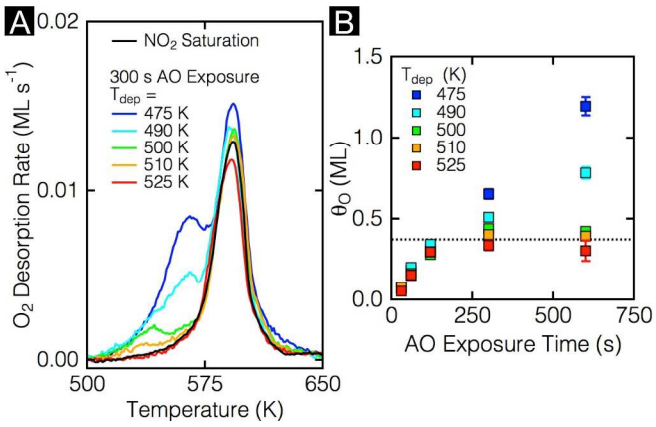


**Figure 3**: A) TPD spectra after 300 s AO exposures at various $T_{dep}$. The black trace is for $\theta_O$ = 0.375 ML from a saturation $NO_2$ exposure and shows that the peak at 595 K corresponds to the decomposition of the surface oxide. The $O_2$ desorption peak below 575 K increases with decreasing temperature and is caused by the emergence and recombinative desorption of $O_{sub}$ to $O_2$. B) Plot of the total amount of O ($O_{ad}$ and $O_{sub}$, $\theta_O$) versus AO exposure time for several $T_{dep}$. For $T_{dep}$ above 500 K, only surface bound O was observed ($\theta_O \leq 0.375$ ML, dashed line), but for lower $T_{dep}$ $\theta_O$ exceeded what was present in the surface oxide.

**Figure 4**

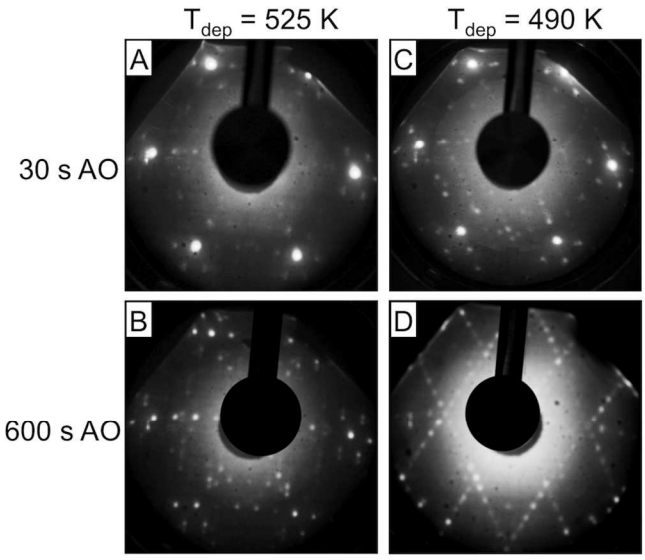


**Figure 4:** Photos of the LEED patterns (all at 52 eV) showing evolution of the surface structure after 30 s and 600 s AO exposures for $T_{dep}$ = 525 K (A and B) and 490 K (C and D). After a 30 s exposure, the patterns were very similar for both temperatures (A and C), but faint rows appeared for $T_{dep}$ = 490 K (C). (B) After a 600 s exposure, the pattern was very similar for $T_{dep}$ = 525 K, but for $T_{dep}$ = 490 K only rows of spots were observed (D).

**Figure 5**

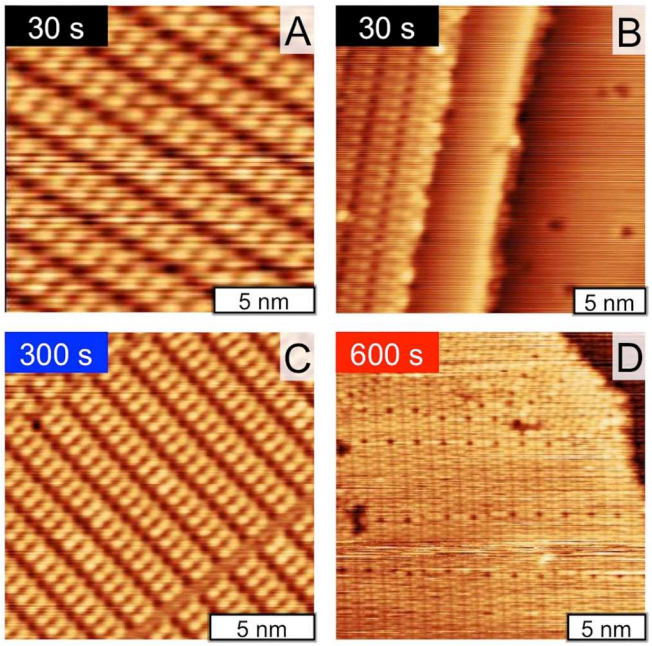


**Figure 5:** STM images of Ag(111) after exposure to AO at $T_{dep}$ = 525 K. Exposure duration is labeled in the upper left corner of each image, and a 5 nm scale bar is in the lower right corner. The p(4×5√3) domain was evident in all images; (A and B) after brief (< 120 s) exposures, areas of clean Ag(111) with isolated O adatoms were observed as black depressions as shown in the upper right-hand image. Imaging conditions for each image were $i$ = 300 pA and $V$ = 900 mV, except for B) which was obtained with $V$ = 1.1 V.

**Figure 6**

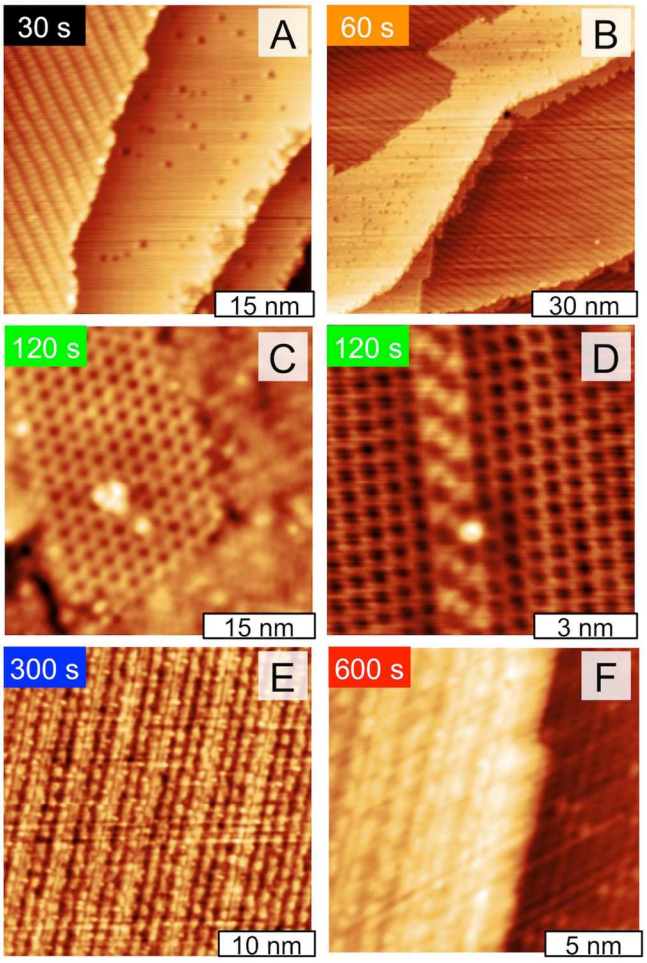


**Figure 6:** STM images of Ag(111) after exposure to AO at $T_{dep}$ = 490 K. Exposure duration is labeled in the upper left corner of each image, and the scale bar is in the lower right corner. A and B) The p(4×5√3) domain was predominant after brief exposures as were areas of clean Ag(111) with isolated O adatoms that were observed as black depressions as shown in the upper right-hand image. C-F) With increasing AO exposure, several domains coexisted until the surface became uniformly covered in the striped pattern after 300 s and 600 s exposures. Imaging conditions for each image (clockwise from upper left) were A) $i$ = 280 pA, $V$ = 1.0 V; B) $i$ = 300 pA, $V$ = 800 mV; C) $i$ = 260 pA, $V$ = 0.400 mV; D) $i$ = 200 pA, $V$ = 800 mV; E) $i$ = 300 pA, $V$ = 900 mV; F) $i$ = 260 pA, $V$ = 0.970 mV.

## TOC Graphic

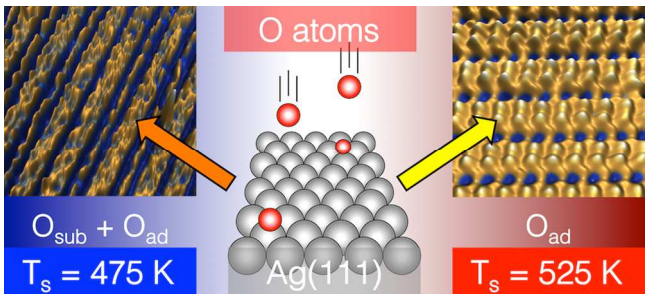

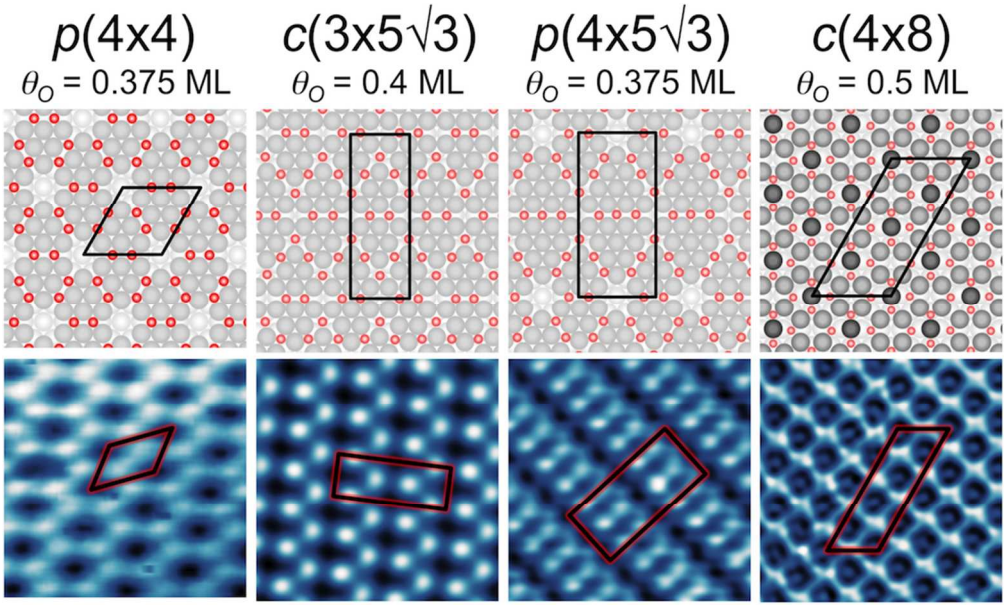


Figure 1: Illustrations of the four principal surface oxide reconstructions observed. From left to right, p(4×4)-O, c(3×5√3)-O, p(4×5√3)-O, and c(4×8)-O. In each illustration, red balls depict O atoms, darker gray the surface Ag atoms, and the light gray balls depict the topmost layer of the underlying Ag(111). Beneath each illustration is a 5 nm × 5 nm STM image of the corresponding surface. Surface unit cells are shown by black tetragons.
85x51mm (300 x 300 DPI)

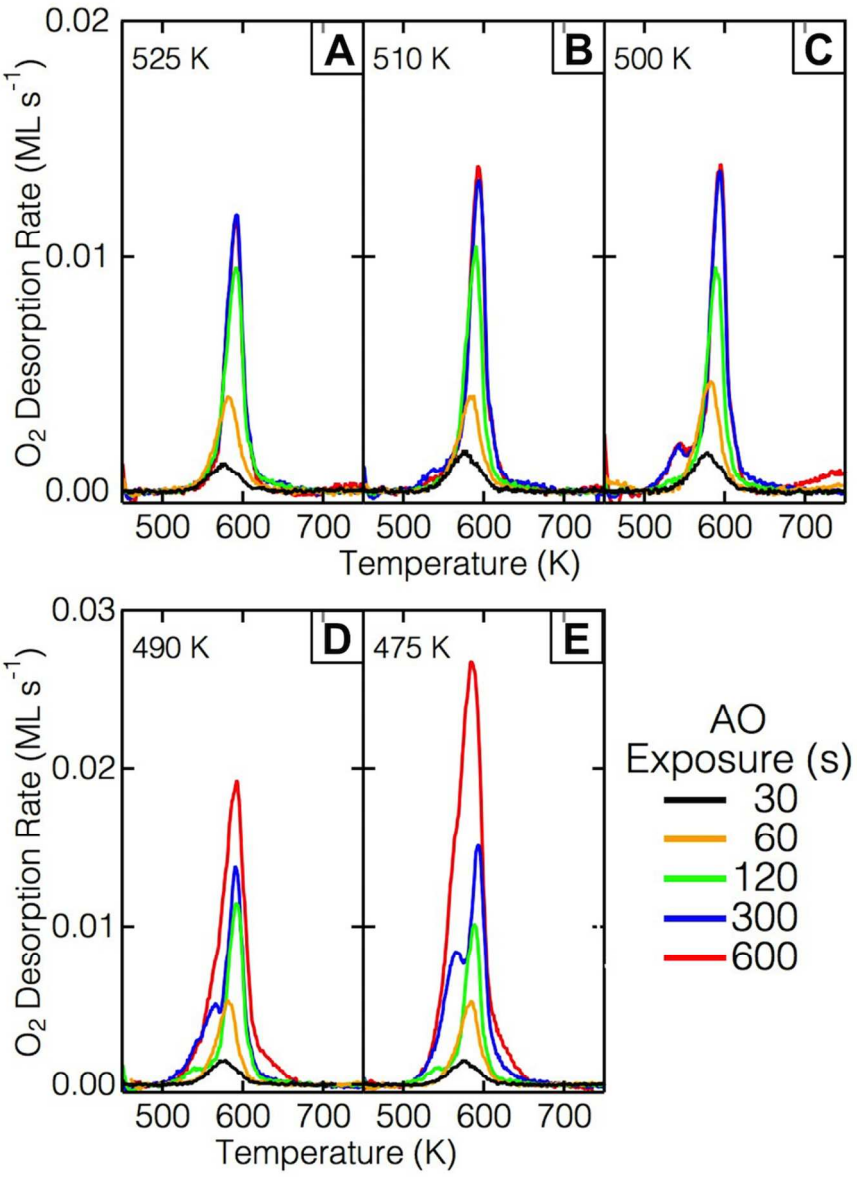


Figure 2: TPD spectra after exposure of Ag(111) to AO at five different temperatures, A) Tdep = 525 K, B) Tdep = 510 K, C) Tdep = 500 K, D) Tdep = 490 K, and E) Tdep = 475 K . For each, the Ir filament was at 1750 K and the background pressure of O2 was 5.0 ×10-7 Torr. The surface oxide peak at 595 K saturates after 300 s (blue traces) for all Tdep, but the lower temperature peak near 550 K increases with exposure time for Tdep below 500 K.
85x118mm (300 x 300 DPI)

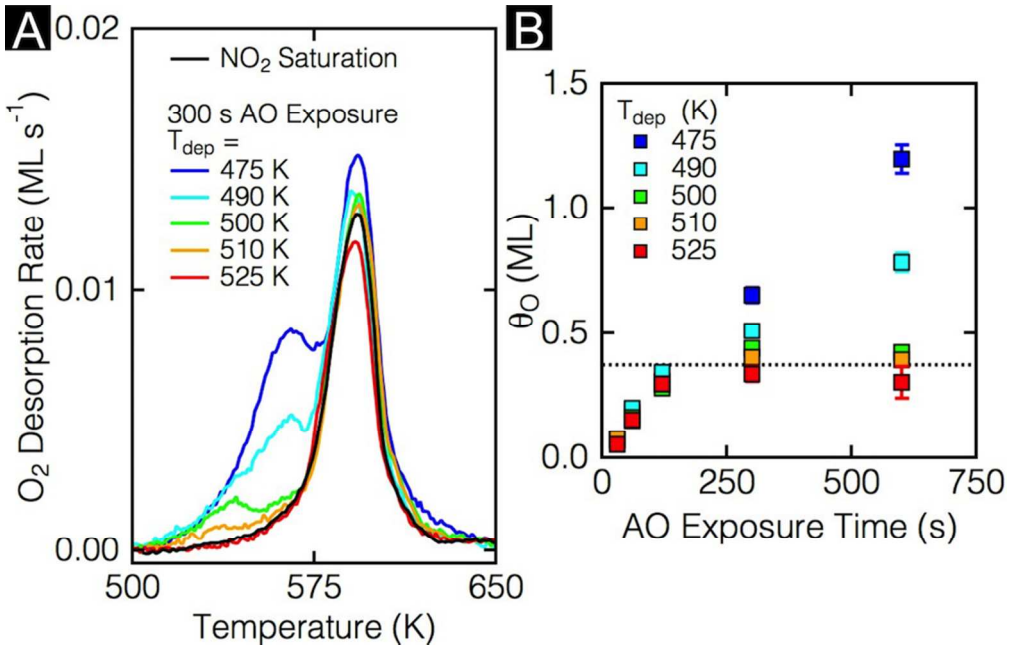


Figure 3: A) TPD spectra after 300 s AO exposures at various Tdep. The black trace is for θO = 0.375 ML from a saturation NO2 exposure and shows that the peak at 595 K corresponds to the decomposition of the surface oxide. The O2 desorption peak below 575 K increases with decreasing temperature and is caused by the emergence and recombinative desorption of Osub to O2. B) Plot of the total amount of O (Oad and Osub, θO) versus AO exposure time for several Tdep. For Tdep above 500 K, only surface bound O was observed (θO ≤ 0.375 ML, dashed line), but for lower Tdep θO exceeded what was present in the surface oxide.
85x54mm (300 x 300 DPI)

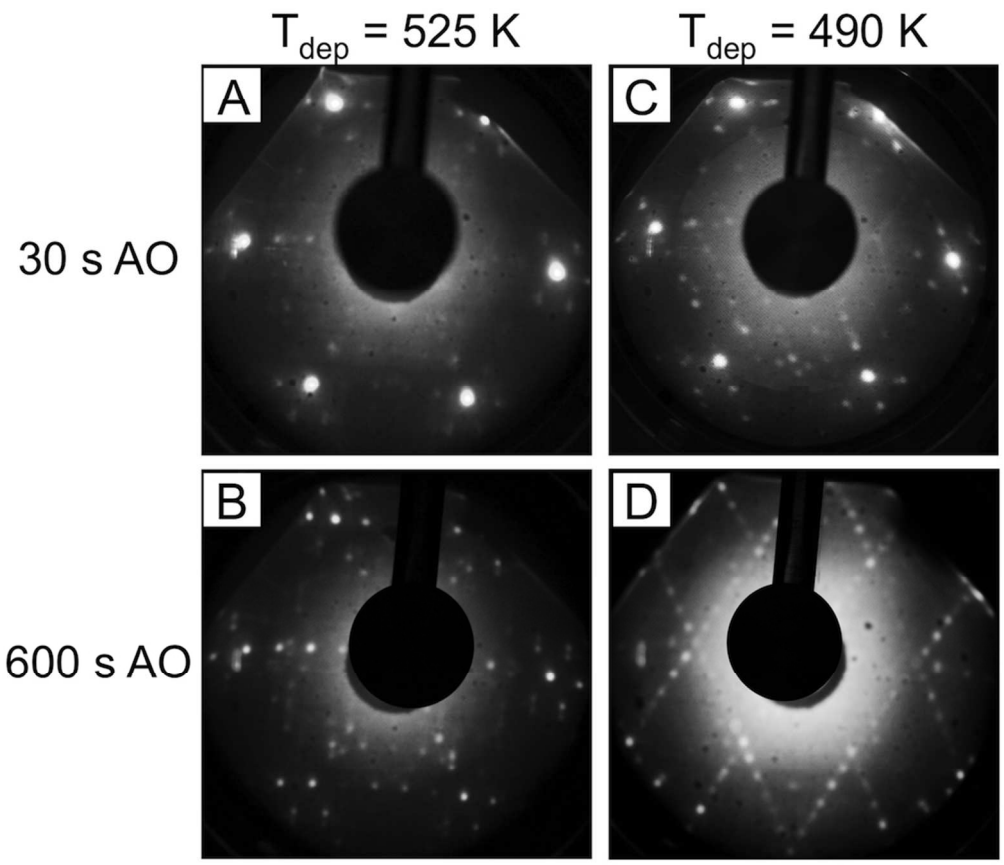


Figure 4: Photos of the LEED patterns (all at 52 eV) showing evolution of the surface structure after 30 s and 600 s AO exposures for Tdep = 525 K (A and B) and 490 K (C and D). After a 30 s exposure, the patterns were very similar for both temperatures (A and C), but faint rows appeared for Tdep = 490 K (C). (B) After a 600 s exposure, the pattern was very similar for Tdep = 525 K, but for Tdep = 490 K only rows of spots were observed (D).
85x73mm (300 x 300 DPI)

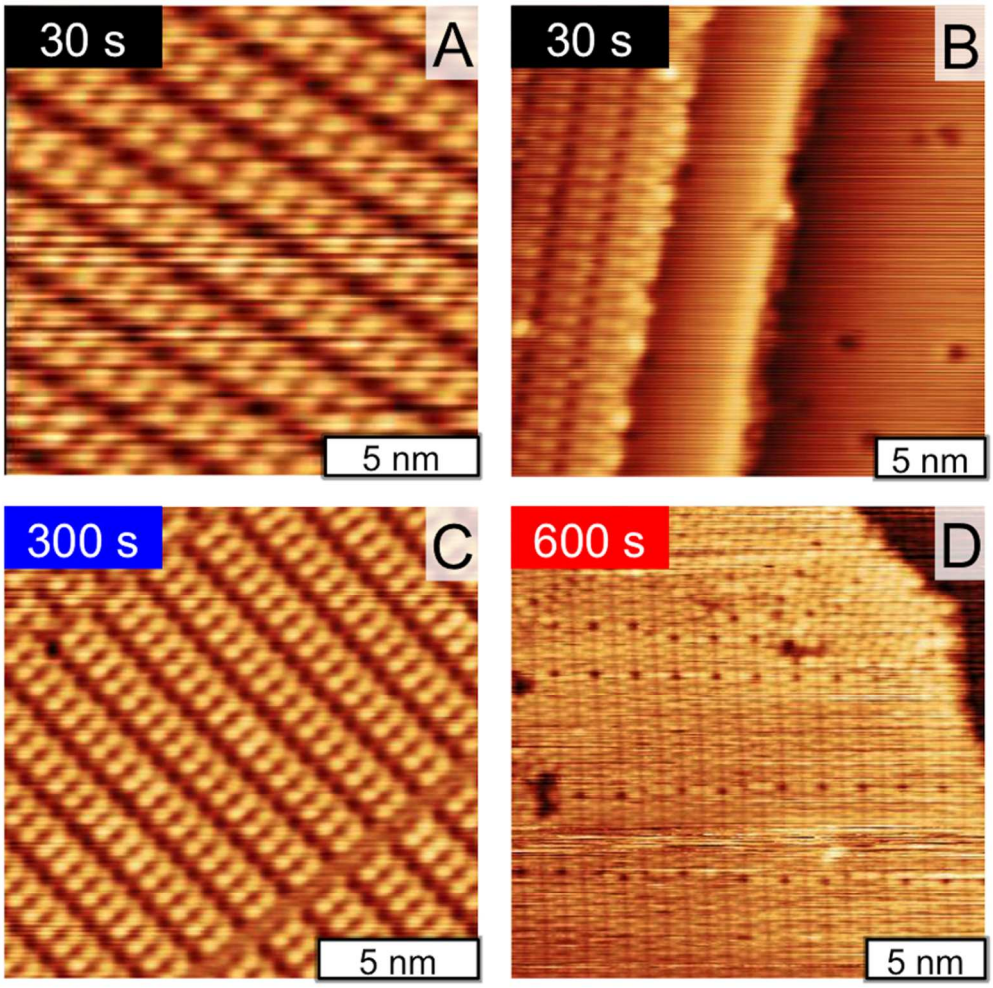


Figure 5: STM images of Ag(111) after exposure to AO at Tdep = 525 K. Exposure duration is labeled in the upper left corner of each image, and a 5 nm scale bar is in the lower right corner. The p(4×5√3) domain was evident in all images; (A and B) after brief (< 120 s) exposures areas of clean Ag(111) with isolated O adatoms were observed as black depressions as shown in the upper right-hand image. Imaging conditions for each image were i = 300 pA and V = 900 mV, except for B) which was obtained with V = 1.1 V.
85x84mm (300 x 300 DPI)

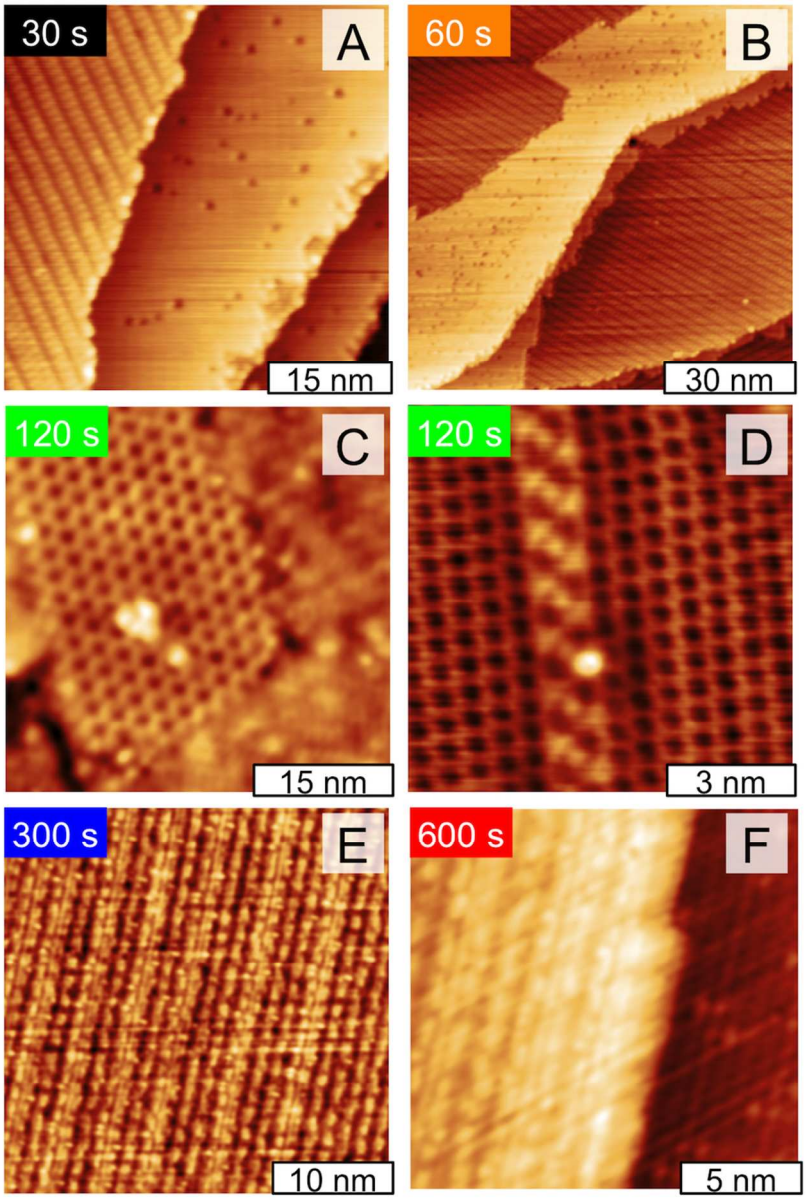


Figure 6: STM images of Ag(111) after exposure to AO at Tdep = 490 K. Exposure duration is labeled in the upper left corner of each image, and the scale bar is in the lower right corner. A and B) The p(4×5√3) domain was predominant after brief exposures as were areas of clean Ag(111) with isolated O adatoms that were observed as black depressions as shown in the upper right-hand image. C-F) With increasing AO exposure, several domains coexisted until the surface became uniformly covered in the striped pattern after 300 s and 600 s exposures. Imaging conditions for each image (clockwise from upper left) were A) i = 280 pA, V = 1.0 V; B) i = 300 pA, V = 800 mV; C) i = 260 pA, V = 0.400 mV; D) i = 200 pA, V = 800 mV; E) i = 300 pA, V = 900 mV; F) i = 260 pA, V = 0.970 mV.
85x126mm (300 x 300 DPI)

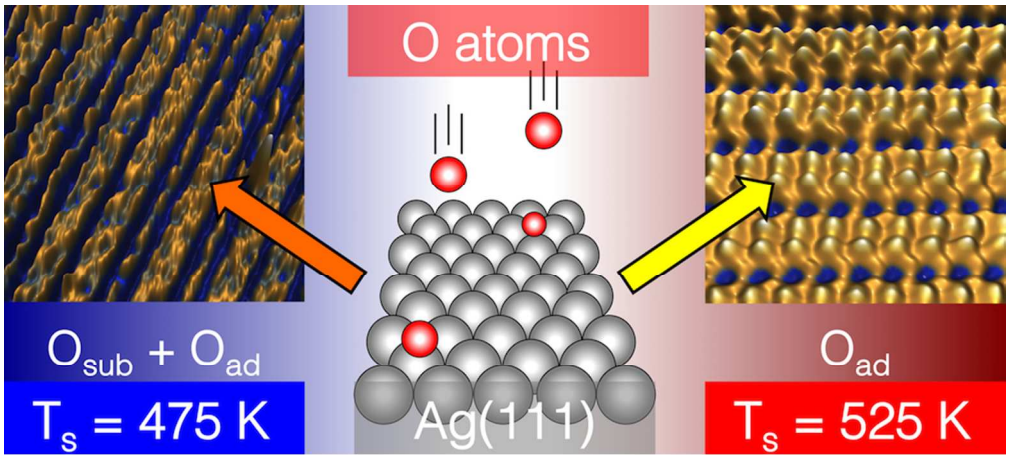


TOC graphic
84x38mm (300 x 300 DPI)